iScience

CellPress
OPEN ACCESS

Article

Macroscopic negative differential thermal resistance in the overlapping graphene homojunction structure

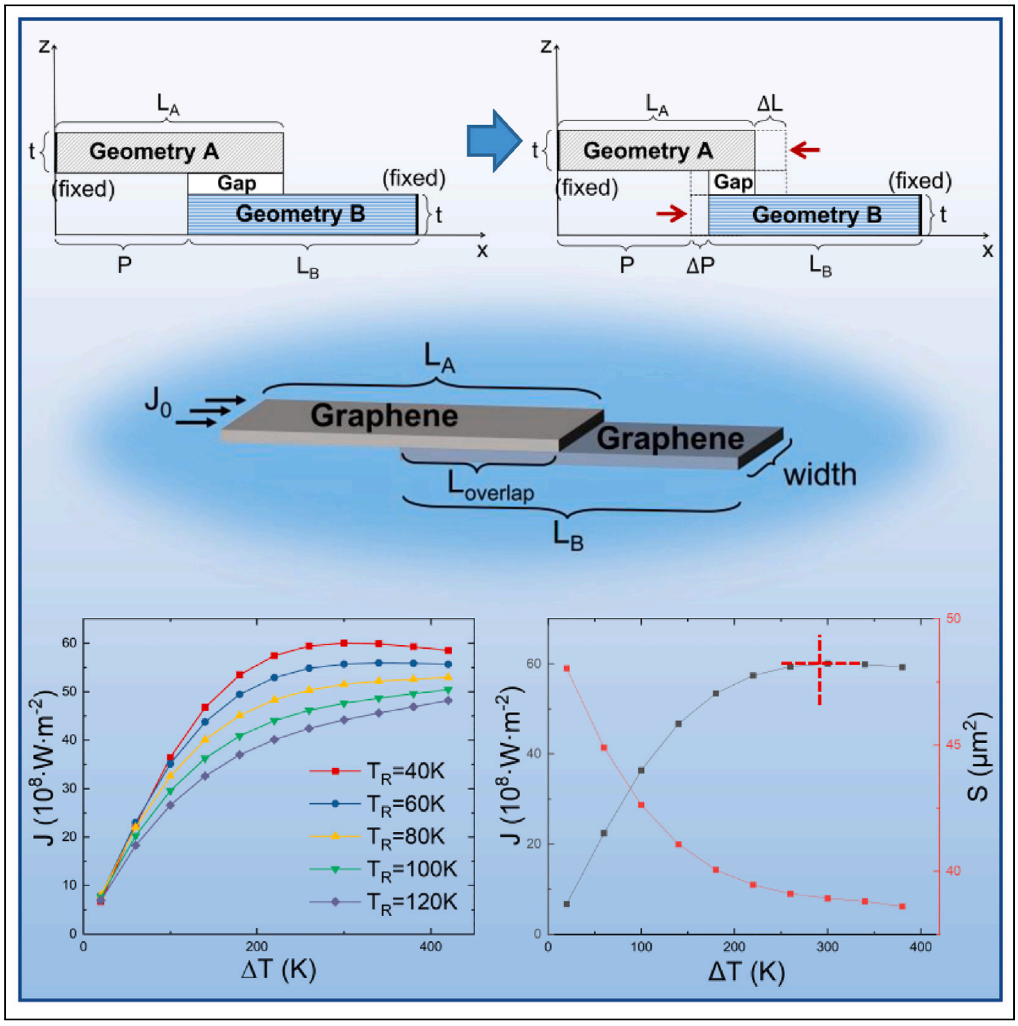

Rui Wu, He Tian, Zhengqiang Zhu, Yanming Liu, Chao-Yang Xing, Gang Zhang, Tian-Ling Ren

tianhe88@tsinghua.edu.cn (H.T.)
zhangg@ihpc.a-star.edu.sg (G.Z.)
RenTL@tsinghua.edu.cn (T.-L.R.)

Highlights

The overlapping graphene homojunction (OGH) model is proposed

It utilizes the thermal properties of graphene, to realize the macroscopic NDTR

The mathematics of OGH Model and an iterative calculation method are proposed

The macroscopic NDTR realization is instructive for further experimental verification

Wu et al., iScience 26, 107493
August 18, 2023
https://doi.org/10.1016/j.isci.2023.107493

iScience

CellPress
OPEN ACCESS

Article

Macroscopic negative differential thermal resistance in the overlapping graphene homojunction structure

Rui Wu,[1,4] He Tian,[1,4,5,*] Zhengqiang Zhu,[1,2,4] Yanming Liu,[1,2,4] Chao-Yang Xing,[2] Gang Zhang,[3,*] and Tian-Ling Ren[1,*]

SUMMARY

As one of the most potential ways to manipulate heat, thermal functional devices have achieved several breakthroughs in recent years, but are still limited to theoretical simulations. One of its theoretical bases is the existence of the negative differential thermal resistance (NDTR). However, most of the existing systems where the phenomenon of NDTR is found are atomic-level systems. In order to realize the macroscopic NDTR and provide effective theoretical guidance and support for the practical realization of thermal functional devices, we construct the overlapping graphene homojunction model, using the negative thermal expansion property of graphene to modify the overlapping area, and thus regulating the heat flow. The COMSOL-MATLAB co-simulation is used to perform calculations through negative feedback loops. It is found that the NDTR phenomenon exists under certain parameter conditions, which can provide new ideas and bring more opportunities for the experimental realization of nonlinear thermal functional devices.

INTRODUCTION

The invention of devices that control the electric current, such as diodes[1–3] and transistors,[4–6] stimulated enormous and comprehensive development in the field of electricity and witnessed the stage transition to modern electronics. Correspondingly, the intention to control the heat flow,[7] another basic energy transport phenomenon and fundamental energy transfer tool, through the control of phonons has aroused great interest. Also, with the integration and miniaturization of electronic devices, heat dissipation has become one of the biggest bottlenecks restricting the development of microelectronics industry.[8–10] It is of great importance to solve the problem of heat dissipation and realize the control of heat flow. Based on this idea, in the 21st century, thermal functional devices have entered a new era of rapid growth and extensive development, with new concepts such as thermal diodes,[11,12] thermal transistors,[13–15] thermal logic gates,[16,17] and thermal memory[18,19] springing up. Similar to electronics transistors, one of the crucial factors for the realization of thermal functional devices is the existence of nonlinearity, specifically, the existence of the negative differential thermal resistance (NDTR) effect.

Traditionally, Fourier's law is widely used in describing macroscopic heat transport, which provides the general concept that the heat flux always increases with temperature gradient increases. On the contrary, NDTR is an anomalous heat conduction phenomenon; it refers to the phenomenon that the heat flux decreases as the temperature gradient increases.[20] It can also be understood from a more intuitive perspective that the phenomenon of NDTR originates from the increasing interfacial thermal resistance (ITR) as the temperature gradient across the interface becomes larger.[21] In other words, it comes from the competition between the promotion of heat flux stemming from the increase of temperature gradient, and the hindrance of heat flux due to the rise in the thermal resistance when a larger temperature difference occurs. The NDTR effect is an interesting counter-intuitive phenomenon. The nonlinearity it embodies brings great possibilities for its further applications and the construction of nonlinear devices.[13,22]

Previous studies about structures with proved existence of the NDTR effect mostly rely on ultra-strong phonon anharmonicity or artificial model,[23–27] which adds the difficulty to the experimental realization of thermal functional devices. Therefore, realization of the NDTR effect in the classical macroscopic system

[1]School of Integrated Circuit and the Beijing National Research Center for Information Science and Technology (BNRist), Tsinghua University, Beijing 100084, China

[2]Beijing Institute of Aerospace Control Devices, Beijing 100094, China

[3]Institute of High Performance Computing, A*STAR, Singapore 138632, Singapore

[4]These authors contributed equally

[5]Lead contact

*Correspondence: tianhe88@tsinghua.edu.cn (H.T.), zhangg@ihpc.a-star.edu.sg (G.Z.), RenTL@tsinghua.edu.cn (T.-L.R.)

https://doi.org/10.1016/j.isci.2023.107493

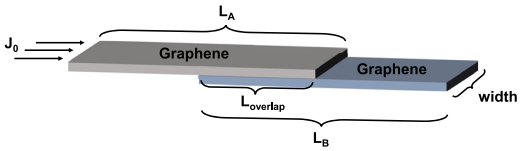

Figure 1. Geometrical structure of the macroscopic overlapping graphene homojunction model, where L_A and L_B are the length of graphene layers, $L_{overlap}$ is the length of the overlapping area, and J_0 is the heat flux in the structure

is of crucial significance to the development of its practical applications. In 2020, Yu et al.[21] simulated materials with known negative thermal expansion coefficients in a homojunction structure to introduce the negative dependency relation between the thermal resistance and the pressure at the interface, thus achieving the NDTR effect at a macro level. However, the negative pressure might disintegrate the homojunction structure and more macroscopic structures are expected.

In this study, an overlap structure of graphene homojunction is proposed, utilizing the negative thermal expansion coefficient of graphene, to realize the macroscopic NDTR effect. In overlapping graphene homojunction model, the overlapping graphene homojunction model is illustrated, including its geometrical structure, its boundary conditions, and the thermal properties of graphene. Next, theoretical derivation is conducted, calculating the length change of the graphene material, which is main cause of the heat flux hindering factor leading to the NDTR phenomenon. Finally, the simulation method is explained and the results are discussed. The analysis of this graphene homojunction structure could be instructive for attempts to find the NDTR experimentally and may reveal new opportunities and possibilities to realize the thermal function devices.

Overlapping graphene homojunction model

As stated previously, the appearance of the NDTR phenomenon, which is contrary to intuition that the heat flux is positively correlated with the temperature gradient, stems from the factor that hinders the heat flow in the entire structure. This factor is expected to exacerbate (which means to impede the heat flux more strongly) with the increase of the temperature difference between two heat sources to counteract a natural heat flow rise in this condition. As a result, the entire structure could have a tendency of increasing temperature gradient and decreasing heat flow. Therefore, it is clear that when looking for the NDTR effect at the macro scale, it is crucial to find a factor that resists the heat flow in the coarse-scaled structure, and that could present a generalized positive correlation with the increasing temperature gradient.

In this work, the negative thermal expansion coefficient of graphene is utilized as the hindering factor. The specific implementation method is to partially overlap two graphene layers to form a macroscopic homojunction structure, named the overlapping graphene homojunction (OGH) model. Its geometrical structure is shown in Figure 1. The size of the graphene layers in this model is in the micrometer scale.

Interfacial and boundary conditions

Since the model is constructed by two overlapped two-dimensional graphene layers, an ITR will inevitably occur at the interface, which leads to a temperature jump between the upper and lower surfaces, as shown in Figure 2A. In order to better describe the produced temperature step, a geometric body is inserted between the two contact surfaces in the OGH model, called the gap layer (Figure 2B).[21] The gap layer satisfies the heat conduction formula of general solids, and its upper and lower surfaces will produce a temperature difference which substitutes the effect of the thermal resistance at the interface. It should be emphasized that the gap layer is merely an equivalent product in the model whose purpose is to simulate the ITR more conveniently, and that its thickness is zero in real geometrical structure. In other words, the gap layer takes the advantage of the temperature difference generated by its geometry to simulate the existence of imperfect interlayer contacts. Thus, perfect contact condition should be set on the interfaces between the gap layer and others in this model. Two heat sources are connected to the left and right ends where fixed displacement boundary conditions are set.

The working mechanism of the OGH model is as follows (Figure 3): when the temperature difference rises, the length of the graphene layers is shortened. Since the two ends of the model are fixed, a smaller overlapping interfacial area will appear, which hinders the heat flow. This hindering factor counteracts the increasing heat flow caused by the increased temperature gradient across the plane. When the factor prevails, the NDTR phenomenon will occur.

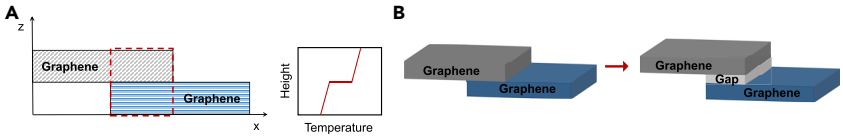

Figure 2. Illustration of interfacial conditions and the modeling method

(A) Figure on the left is a longitudinal section of the model. The simplified temperature distribution of the part circled by the red dashed box is shown on the right. A temperature jump (displayed as horizontal line) occurs at the interface of two graphene layers induced by the ITR.[21]

(B) A gap layer is constructed in the model. It is a hypothetical layer for the convenience of calculation, representing the interface.

Thermal properties of graphene

Monolayer graphene, a two-dimensional material with various unique characteristics and long-term widespread attention,[8,28–31] is chosen here because of its negative thermal expansion coefficient (TEC).[32–34]

The negative TEC of graphite has been known to scientists since the 1940s,[35] which remains negative in the temperature range of 0–700 K.[36] After the graphene was first obtained by the mechanical exfoliation in 2004,[37] the research of its TEC was quickly carried out using the first-principles calculations.[33] But even until 2008, when the thermal conductivity of single-layered graphene was measured for the first time, the thermal expansion characteristics of graphene had not yet been clearly supported by experimental data.[38] In 2009, Bao et al.[39] conducted the first experimental measurement of the TEC of suspended monolayer graphene, and obtained the result of $\boldsymbol{\alpha} = -7 \times 10^{-6}\ K^{-1}$ at 300 K. Now, there are many related studies on the theoretical derivation and experimental measurement of graphene's thermal expansion coefficient,[34,40–44] and it is still one of the research fields that attract much attention.[45–47]

In this work, the coefficient is selected from the experiment results in Bao et al.'s study.[39] A polynomial fitting of the graphene's TEC given in this literature is performed, and the result is shown in Figure 4A. The fitted thermal expansion coefficient is expressed as:

$$\alpha(T) = -9.37\cdot10^{-4} + 7.25\cdot10^{-6}T - 1.856\cdot10^{-8}T^2 + 1.639\cdot10^{-11}T^3 \quad (K^{-1})$$

Research on graphene's high in-plane thermal conductivity (TC) has been underway for more than a decade. The thermal conductivity of graphene is well studied,[49] which could be affected by various factors such as sample length,[50,51] number of layers,[52–54] defects,[55–58] doping,[59–62] etc. The thermal conductivity of graphene discussed in this paper is taken between 1500 and 3500 $W/(m\cdot K)$.[49,50]

Graphene has an anisotropic thermal conductivity, which is ultrahigh in plane, but rather low in the direction perpendicular to the plane.[63–65] This is because only weak van der Waals forces exist between the layers.[66,67] A previous study described the relation between the temperature and the graphite's TC in the cross-plane direction,[48] which could be used as an estimation of the TC vertical to the interface in our graphene homojunction structure. The fitting results are shown in Figure 4B.

Derivation of theory model

This section uses the thermal expansion coefficient of graphene obtained in section thermal properties of graphene to calculate the change of graphene layer's length under a specific temperature distribution. Considering the simplicity of the calculation and the programming process, the derivation mainly uses the numerical calculation method of Gaussian quadrature.[68]

The basic calculation formula of thermal expansion coefficient and strain is shown as follows:

$$\varepsilon = \int_{T_0(x)}^{T(x)} \alpha(T)dT = \frac{du}{dx},$$

where $\alpha(T)$ is the fitting result of the TEC of the graphene material, $T_0(x)$ is the initial temperature value at the position x, $T(x)$ is the temperature value after temperature change, and ε represents the caused length variation on the length dx.

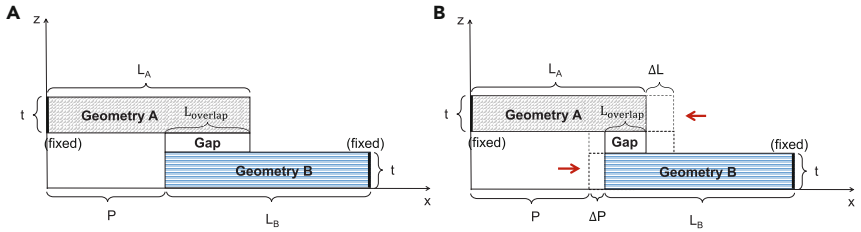

Figure 3. Illustration of the deformation mechanism when the temperature gradient increases, serving as a hindering factor of heat flux, where geometry (A) and (B) indicate the graphene layers

For the upper layer of graphene, when the temperature distribution changes from T_0 to T, the total length variation can be calculated as follows:

$$\Delta L = \int_0^{L_A} du = \int_0^{L_A} \varepsilon dx = \int_0^{L_A} \int_{T_0(x)}^{T(x)} \alpha(T) dT dx.$$

where L_A is the length of the upper-layer graphene.

Because Gaussian quadrature handles integration over a symmetrical parameter range,[69] a linear transformation is conducted to map the independent variable to the interval [-1, 1]:

$$x = \frac{1}{2}L_A + \frac{1}{2}L_A\xi$$

$$dx = \frac{1}{2}L_A d\xi$$

Let $g(x) = \int_{T_0(x)}^{T(x)} \alpha(T) dT$. By implementing Gaussian quadrature, the length variation expression can be written as:

$$\Delta L = \int_0^{L_A} g(x) dx = \frac{1}{2}L_A \int_{-1}^{1} g(\xi) d\xi = \frac{1}{2}L_A \widehat{I_1},$$

$$\widehat{I_1} = \omega_1 g(\xi_1) + \omega_2 g(\xi_2) + \cdots + \omega_n g(\xi_n),$$

where ξ_i are the interior points and ω_i are the corresponding weights, approximating the integral value by a weighted sum.

Under a specific ξ_i and ω_i value, performing similar coordinate transformation $dT = \frac{1}{2}[T(\xi_i) - T_0(\xi_i)]d\eta$, the function is derived as:

$$g(\xi_i) = \frac{1}{2}[T(\xi_i) - T_0(\xi_i)] \int_{-1}^{1} \alpha(\eta) d\eta = \frac{1}{2}[T(\xi_i) - T_0(\xi_i)]\widehat{I_2},$$

$\widehat{I_2}$ can be calculated by the same method used before, leveraging the formula of graphene's TEC.

Let the degree of the polynomial $f(x)$ be $N[f(x)]$ and it could be derived from above that,

$$N[g(x)] = \{N[\alpha(x)] + 1\} \times N[T(x)]$$

It is known that an n points Gaussian quadrature can accurately yield the value of the integral of a 2n-1° polynomial. Therefore, the number of Gaussian points taken by the two Gaussian integrals should be $N_1 = 3, N_2 = 2$.

A similar calculation method could be implemented to the lower layer of graphene. The length of the gap layer varies with the graphene layers.

Numerical simulation of the OGH model

Since the length of the graphene layers is simultaneously changing with the temperature distribution, which in turn changes with the overlapping area, the method of iterative simulation with a negative

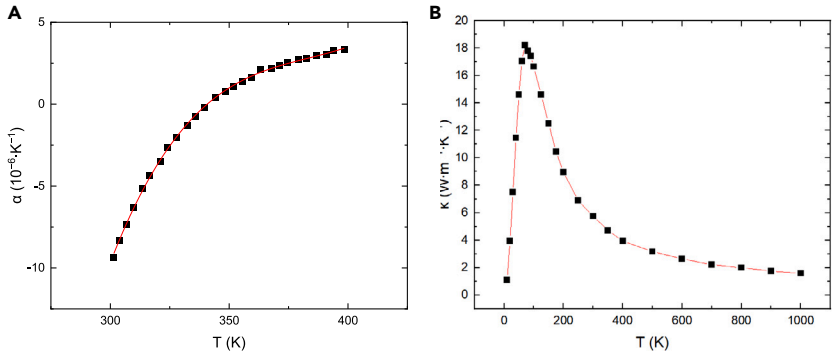

Figure 4. Thermal properties (TEC and TC) of graphene material

(A) Polynomial fitting (red line) of the graphene's thermal expansion coefficient-temperature curve. The black dots are data collected from previous experimental measurement.[39]

(B) Fitting diagram (red line) of the thermal conductivity cross the graphene layers with temperature change. Black dots are data collected from Pop et al.[48]

feedback loop is adopted here to solve the problem. The process is mainly divided into three steps. ***Step1:*** Given the temperature of two heat sources on the left and right ends, finite element method (FEM) is used to calculate the overall temperature distribution in the graphene's overlapping structure. ***Step 2:*** Through the numerical approximation in derivation of theory model, the length change of the graphene layers under the current temperature profile can be obtained. Substitute the updated length into the model to continue calculation by FEM and obtain a new temperature distribution. ***Step 3:*** Repeat the second step until the length of the graphene layers steadily converges to a fixed value. Through this iterative method, the negative thermal expansion coefficient of graphene could be successfully taken into consideration and the heat flow in the model under a specific temperature distribution can be obtained in the simulation.

RESULTS AND DISCUSSIONS

The COMSOL Multiphysics and MATLAB software are used to calculate the thermal flow at a nonequilibrium stationary state under different temperature differences. After the simulation, the NDTR phenomenon in the OGH model is found for the first time when the temperature of the low-temperature heat source is 40 K, the initial length is 15 μm, and the in-plane thermal conductivity is set as 3000 $W/(m \cdot K)$. Figure 5A shows the relationship between the value of the heat flow, the overlapping area in the model, and the temperature difference between the cold and hot ends. It could be found that the turning point of the heat flow occurs when the temperature difference is 290K. After this point (as the red dash lines indicate), $dJ(T)/d\Delta T \nleq 0$, a negative differential thermal resistance phenomenon appears.

When the low temperature heat source (here, the right end of the model) takes different values, the thermal response generated by the OGH model will change accordingly. As shown in Figure 6A, when the temperature at the right end is taken as 40 K, the phenomenon of NDTR appears in the homojunction, while the heat flow does not decrease with the increase of the temperature difference when T_R is higher. In addition, it could be noted from the figure that when the overall temperature is lower, the heat flow in the structure will be slightly higher. This is mainly because under this condition, the lower the T_R, the higher range the interlayer thermal conductivity will fall within, resulting in greater heat flow in the structure. Furthermore, in the selected temperature range, the lower the temperature is, the larger the absolute value of the negative TEC is, so the overlapping area is correspondingly smaller, as shown in Figure 6B. It should be emphasized that the gap layer is merely an equivalent product in the model whose purpose is to simulate the ITR more conveniently and that its thickness is zero in real geometrical structures. In other words, the gap layer takes the advantage of the temperature difference generated by its geometry to simulate the existence of imperfect interlayer contacts. The thickness of the gap layer will actually affect the eventual results of NDTR for it is only a mathematical model (Figure 6C). The TC of the gap layer should also be adjusted for satisfied the self-consistency of the model as the thickness of the gap layer is changed. Moreover, perfect contact conditions should be set on the interfaces between the gap layer and others in this model. Two heat sources are connected to the left and right ends where fixed displacement boundary conditions are set.

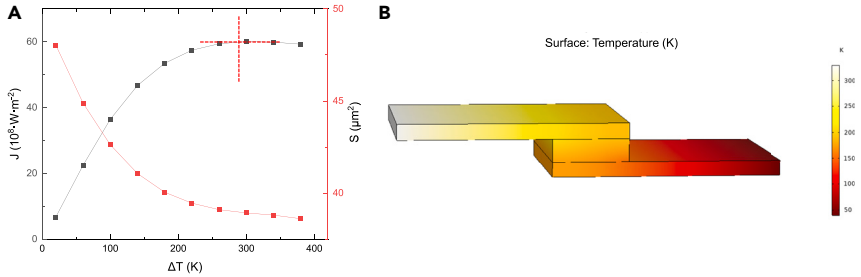

Figure 5. Appearance of the NDTR phenomenon in the OGH model

(A) The relation between the heat flow *J*, the temperature difference Δ*T*, and the overlapping area *S*. The red dash lines indicate the point when the heat flow no longer grows with the increase in the temperature difference.

(B) An illustration of the temperature distribution in the OGH model.

The effect of other parameter variations on the appearance of the NDTR phenomenon is further discussed. When the in-plane thermal conductivity of graphene in the model is changed, we obtain the results shown in Figure 7A. It is found that a relatively lower in-plane thermal conductance results in an overall smaller heat flow. And as the thermal conductivity decreases, the temperature difference required for the NDTR phenomenon to appear tends to increase. The thermal conductivity across the graphene layers also affects the simulation results. By multiplying a constant coefficient c on the TC value obtained from the previous paper,[48] the interlayer thermal conductivity is changed as shown in Figure 7B. It can be seen from the figure that a small cross-plane TC will accelerate the appearance of NDTR effect, that is, it tends to appear when the temperature difference is smaller. It could be understood from the perspective that the smaller TC amplifies the hindering effect on the heat flow caused by the reduction of the overlapping area. In addition, graphene follows different heat conduction mechanisms in-plane and cross-plane. Heat transfer is by covalent bonds (atomic bonds) within the in-plane graphene and van der Waals force (molecular bonds) between the cross-plane graphene, which is also the reason of this phenomenon. This conclusion is favorable for future experimental verification, because due to the influence of defects, imperfect contact and other factors, the thermal conductivity between layers is usually smaller than expected. Changing the initial length of graphene, that is, changing the initial overlapping area of the upper and lower graphene layers, can also affect the simulation results. Figure 7C shows the effect of different initial lengths on the heat flow in the homojunction. It can be found that when the initial length is shorter, the graphene homojunction structure will exhibit NDTR phenomenon at a smaller temperature difference. It shows that when the initial area is smaller, the thermal response of the structure will be more sensitive to the change in area. This could be valuable for future implementations, enhancing the usability of the experimental model by decreasing the overlapping aera at the beginning. Also, the smaller the overlapping area, the greater the resistance to heat flow, which is reflected as an overall heat flow decrease as the length decreases. In addition, the thermal effect of this structure is sensitive to the change of length, which also verifies the rationality of choosing to use the negative TEC to change the overlapping area to manipulate the heat flow.

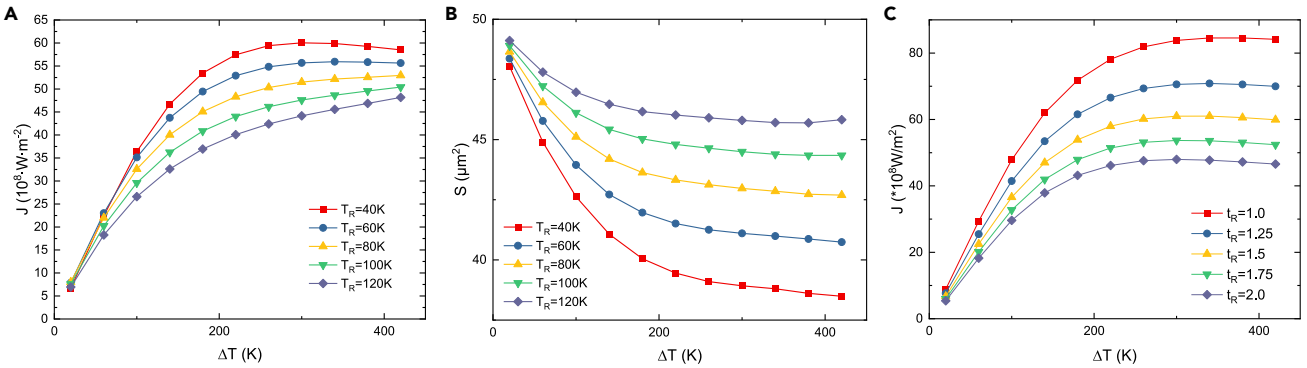

Figure 6. Factors that affect the thermal responses of the model and the appearance of the NDTR phenomenon

(A) The relationship between the heat flow and the temperature difference between two heat sources when the low-temperature heat source takes different values.

(B) The relationship between the overlapping area and the temperature difference when the low-temperature heat source takes different values.

(C) The relationship between the heat flow and the temperature difference when the thickness of gap layer takes different values.

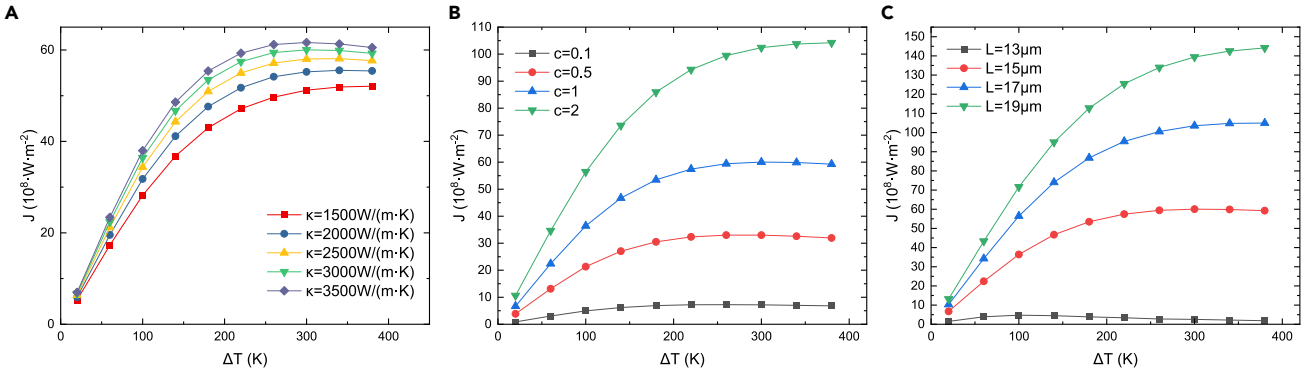

Figure 7. Other factors that may affect the simulation results and the appearance of the NDTR phenomenon

Relationship between the heat flow and the temperature difference with different (A) in-plane thermal conductivity, (B) interlay thermal conductivity, and (C) initial length of graphene. The parameter c in (B) is a constant multiplied with the interlayer TC of graphene.

Conclusion

In summary, we found the existence of NDTR effect in the overlapping graphene homojunction structure, which professes the possibility of NDTR in the macro system. A mathematical and physical model of overlapped graphene and an iterative calculation method are innovatively proposed to simulate the macroscopic NDTR phenomenon. Meanwhile, the mathematical solution of simulation with varying length is derived by MATLAB coding. It is a macroscopic NDTR realization mechanism that may have guiding significance for further experimental verification.

STAR★METHODS

Detailed methods are provided in the online version of this paper and include the following:

- KEY RESOURCES TABLE
- RESOURCE AVAILABILITY
  - Lead contact
  - Materials availability
  - Data and code availability
- METHOD DETAILS
- QUANTIFICATION AND STATISTICAL ANALYSIS

ACKNOWLEDGMENTS

This work was supported in part by STI 2030—Major Projects under grant 2022ZD0209200, in part by National Natural Science Foundation of China under grant 62022047, grant U20A20168, and grant 51861145202, in part supported by Tsinghua University-Zhuhai Huafa Industrial Share Company Joint Institute for Architecture Optoelectronic Technologies (JIAOT) (KF202204), in part by the National Key R&D Program under grant 2016YFA0200400, in part by Fok Ying Tong Education Foundation under grant 171051, in part by Beijing Natural Science Foundation (M22020), in part by the Independent Research Program of Tsinghua University under grant 2022Z11QYJ044, in part by the Tsinghua-Toyota Joint Research Fund, in part by the Daikin-Tsinghua Union Program, in part by State Key Laboratory of New Ceramic and Fine Processing Tsinghua University (No. KF202109); in part by the Opening Project of the Key Laboratory of Microelectronic Devices & Integrated Technology, Institute of Microelectronics, Chinese Academy of Sciences, in part by Independent Research Program of School of Integrated Circuits, Tsinghua University, in part by the Guoqiang Institute, Tsinghua University, and in part by the research fund from Beijing Innovation Center for Future Chip.

AUTHOR CONTRIBUTIONS

Conceptualization, H.T., G.Z., and R.W.; Methodology, R.W., H.T., and G.Z.; Software and Formal Analysis, R.W.; Data Curation, R.W. and Y.L.; Writing – Original Draft, R.W., H.T., and G.Z.; Writing – Review & Editing, H.T., G.Z., Y.L., Z.Z., and C.Y.X.; Funding Acquisition: H.T.; Supervision, H.T., G.Z., and T.L.R.

DECLARATION OF INTERESTS

The authors declare no competing interests.

INCLUSION AND DIVERSITY

We support inclusive, diverse, and equitable conduct of research.

Received: October 4, 2022
Revised: June 15, 2023
Accepted: July 22, 2023
Published: July 27, 2023

REFERENCES

1. Mukunda, D.C., Joshi, V.K., and Mahato, K.K. (2022). Light emitting diodes (LEDs) in fluorescence-based analytical applications: A review. Appl. Spectrosc. Rev. *57*, 1–38. https://doi.org/10.1080/05704928.2020.1835939.

2. Thomas, E.F. (1975). Mechanisms of current induced degradation in a GaAs light emitting diode. In 13th International Reliability Physics Symposium, pp. 215–220.

3. Bergh, A.A., and Dean, P.J. (1976). Light-emitting Diodes. Proceedings of the IEEE *60*, 156–223.

4. Bardeen, J., and Brattain, W.H. (1948). The transistor, a semi-conductor triode. Phys. Rev. *74*, 230–231. https://doi.org/10.1103/PhysRev.74.230.

5. Likharev, K. (1987). Single-electron transistors: electrostatic analogs of the DC squids. IEEE Trans. Magn. *23*, 1142–1145. https://doi.org/10.1109/Tmag.1987.1065001.

6. Kastner, M.A. (1992). The single-electron transistor. Rev. Mod. Phys. *64*, 849–858. https://doi.org/10.1103/RevModPhys.64.849.

7. Li, N., Ren, J., Wang, L., Zhang, G., Hänggi, P., and Li, B. (2012). Colloquium: Phononics: Manipulating heat flow with electronic analogs and beyond. Rev. Mod. Phys. *84*, 1045–1066. https://doi.org/10.1103/RevModPhys.84.1045.

8. Wu, R., Zhu, R.-Z., Zhao, S.-H., Zhang, G., Tian, H., and Ren, T.L. (2021). Filling the gap: Thermal properties and device applications of graphene. Sci. China Inf. Sci. *64*, 140401–140417.

9. Pan, M., Zhong, X., Dong, G., and Huang, P. (2019). Experimental study of the heat dissipation of battery with a manifold micro-channel heat sink. Appl. Therm. Eng. *163*, 114330.

10. Tang, H., Tang, Y., Wan, Z., Li, J., Yuan, W., Lu, L., Li, Y., and Tang, K. (2018). Review of applications and developments of ultra-thin micro heat pipes for electronic cooling. Appl. Energy *223*, 383–400.

11. Wong, M., Tso, C., Ho, T., and Lee, H.H. (2021). A review of state of the art thermal diodes and their potential applications. Int. J. Heat Mass Transf. *164*, 120607.

12. Li, B., Wang, L., and Casati, G. (2004). Thermal diode. Phys. Rev. Lett. *93*, 184301.

13. Li, B., Wang, L., and Casati, G. (2006). Negative differential thermal resistance and thermal transistor. Appl. Phys. Lett. *88*, 143501.

14. Ben-Abdallah, P., and Biehs, S.A. (2014). Near-field thermal transistor. Phys. Rev. Lett. *112*, 044301.

15. Joulain, K., Drevillon, J., Ezzahri, Y., and Ordonez-Miranda, J. (2016). Quantum thermal transistor. Phys. Rev. Lett. *116*, 200601.

16. Wang, L., and Li, B. (2007). Thermal logic gates: Computation with phonons. Phys. Rev. Lett. *99*, 177208.

17. Kathmann, C., Reina, M., Messina, R., Ben-Abdallah, P., and Biehs, S.A. (2020). Scalable radiative thermal logic gates based on nanoparticle networks. Sci. Rep. *10*, 3596–3611.

18. Wang, L., and Li, B. (2008). Thermal memory: A storage of phononic information. Phys. Rev. Lett. *101*, 267203.

19. Guarcello, C., Solinas, P., Braggio, A., Di Ventra, M., and Giazotto, F. (2018). Josephson thermal memory. Phys. Rev. Appl. *9*, 014021.

20. He, D., Buyukdagli, S., and Hu, B. (2009). Origin of negative differential thermal resistance in a chain of two weakly coupled nonlinear lattices. Phys. Rev. B *80*, 104302.

21. Yang, Y., Ma, D., Zhao, Y., and Zhang, L. (2020). Negative differential thermal resistance effect in a macroscopic homojunction. J. Appl. Phys. *127*, 195301.

22. Pereira, E. (2010). Graded anharmonic crystals as genuine thermal diodes: Analytical description of rectification and negative differential thermal resistance. Phys. Rev. E *82*, 040101.

23. Yang, N., Li, N., Wang, L., and Li, B. (2007). Thermal rectification and negative differential thermal resistance in lattices with mass gradient. Phys. Rev. B *76*, 020301.

24. Zhong, W.-R., Yang, P., Ai, B.-Q., Shao, Z.-G., and Hu, B. (2009). Negative differential thermal resistance induced by ballistic transport. Phys. Rev. E *79*, 050103.

25. Yang, N., Zhang, G., and Li, B. (2009). Thermal rectification in asymmetric graphene ribbons. Appl. Phys. Lett. *95*, 033107.

26. Ai, B.-Q., Zhong, W.-R., and Hu, B. (2011). Double negative differential thermal resistance induced by nonlinear on-site potentials. Phys. Rev. E Stat. Nonlin. Soft Matter Phys. *83*, 052102.

27. Li, F., Wang, J., Xia, G., and Li, Z. (2019). Negative differential thermal resistance through nanoscale solid–fluid–solid sandwiched structures. Nanoscale *11*, 13051–13057.

28. Soldano, C., Mahmood, A., and Dujardin, E. (2010). Production, properties and potential of graphene. Carbon N. Y. *48*, 2127–2150.

29. Neto, A.C., Guinea, F., Peres, N.M., Novoselov, K.S., and Geim, A.K. (2009). The electronic properties of graphene. Rev. Mod. Phys. *81*, 109.

30. Falkovsky, L.A. (2008). Optical Properties of Graphene*1* (IOP Publishing), p. 012004.

31. Papageorgiou, D.G., Kinloch, I.A., and Young, R.J. (2017). Mechanical properties of graphene and graphene-based nanocomposites. Prog. Mater. Sci. *90*, 75–127.

32. Yoon, D., Son, Y.-W., and Cheong, H. (2011). Negative thermal expansion coefficient of graphene measured by Raman spectroscopy. Nano Lett. *11*, 3227–3231.

33. Mounet, N., and Marzari, N. (2005). First-principles determination of the structural, vibrational and thermodynamic properties of diamond. Phys. Rev. B *71*, 205214.

34. Shaina, P.R., George, L., Yadav, V., and Jaiswal, M. (2016). Estimating the thermal expansion coefficient of graphene: The role of graphene–substrate interactions. J. Phys. Condens. Matter *28*, 085301.

35. Entwisle, F. (1962). Thermal expansion of pyrolytic graphite. Phys. Lett. *2*, 236–238.

36. Steward, E.G., Cook, B.P., and Kellett, E.A. (1960). Dependence on temperature of the interlayer spacing in carbons of different graphitic perfection. Nature *187*, 1015–1016.

37. Novoselov, K.S., Geim, A.K., Morozov, S.V., Jiang, D., Zhang, Y., Dubonos, S.V., Grigorieva, I.V., and Firsov, A.A. (2004). Electric field effect in atomically thin carbon films. Science *306*, 666–669.

38. Balandin, A.A., Ghosh, S., Bao, W., Calizo, I., Teweldebrhan, D., Miao, F., and Lau, C.N. (2008). Superior thermal conductivity of single-layer graphene. Nano Lett. *8*, 902–907.

39. Bao, W., Miao, F., Chen, Z., Zhang, H., Jang, W., Dames, C., and Lau, C.N. (2009). Controlled ripple texturing of suspended graphene and ultrathin graphite membranes. Nat. Nanotechnol. *4*, 562–566.

40. Singh, V., Sengupta, S., Solanki, H.S., Dhall, R., Allain, A., Dhara, S., Pant, P., and Deshmukh, M.M. (2010). Probing thermal expansion of graphene and modal dispersion at low-temperature using graphene nanoelectromechanical systems resonators. Nanotechnology *21*, 165204.

41. Jiang, J.-W., Wang, J.-S., and Li, B. (2009). Thermal expansion in single-walled carbon nanotubes and graphene: Nonequilibrium Green's function approach. Phys. Rev. B *80*, 205429.

42. Sevik, C. (2014). Assessment on lattice thermal properties of two-dimensional honeycomb structures: Graphene, H-BN, H-MoS2, and h-MoSe2. Phys. Rev. B *89*, 035422.

43. Alamusi, Li, H., Ning, Y., Gu, B., Hu, N., Yuan, W., Jia, F., Liu, H., Li, Y., Liu, Y., et al. (2018). Molecular dynamics simulations of thermal expansion properties of single layer graphene sheets. Mol. Simul. *44*, 34–39.

44. Tian, S., Yang, Y., Liu, Z., Wang, C., Pan, R., Gu, C., and Li, J. (2016). Temperature-dependent Raman investigation on suspended graphene: contribution from thermal expansion coefficient mismatch between graphene and substrate. Carbon N. Y. *104*, 27–32.

45. Lopez-Polin, G., Gomez-Navarro, C., and Gomez-Herrero, J. (2022). The effect of rippling on the mechanical properties of graphene. Nano Mater. Sci. *4*, 18–26.

46. Ho, D.T., Park, H.S., Kim, S.Y., and Schwingenschlogl, U. (2022). Graphene origami with highly tunable coefficient of thermal expansion. ACS Nano *14*, 8969–8974.

47. McQuade, G.A., Plaut, A.S., Usher, A., and Martin, J. (2021). The thermal expansion coefficient of monolayer, bilayer, and trilayer graphene derived from the strain induced by cooling to cryogenic temperatures. Appl. Phys. Lett. *118*, 203101.

48. Pop, E., Varshney, V., and Roy, A.K. (2012). Thermal properties of graphene: Fundamentals and applications. MRS Bull. *37*, 1273–1281.

49. Balandin, A.A. (2011). Thermal properties of graphene and nanostructured carbon materials. Nat. Mater. *10*, 569–581.

50. Nika, D., Ghosh, S., Pokatilov, E., and Balandin, A. (2009). Lattice thermal conductivity of graphene flakes: Comparison with bulk graphite. Appl. Phys. Lett. *94*, 203103.

51. Xu, X., Pereira, L.F.C., Wang, Y., Wu, J., Zhang, K., Zhao, X., Bae, S., Tinh Bui, C., Xie, R., Thong, J.T.L., et al. (2014). Length-dependent thermal conductivity in suspended single-layer graphene. Nat. Commun. *5*, 3689–3696.

52. Malekpour, H., Chang, K.-H., Chen, J.-C., Lu, C.-Y., Nika, D.L., Novoselov, K.S., and Balandin, A.A. (2014). Thermal conductivity of graphene laminate. Nano Lett. *14*, 5155–5161.

53. Jang, W., Chen, Z., Bao, W., Lau, C.N., and Dames, C. (2010). Thickness-dependent thermal conductivity of encased graphene and ultrathin graphite. Nano Lett. *10*, 3909–3913.

54. Ghosh, S., Bao, W., Nika, D.L., Subrina, S., Pokatilov, E.P., Lau, C.N., and Balandin, A.A. (2010). Dimensional crossover of thermal transport in few-layer graphene. Nat. Mater. *9*, 555–558.

55. Zhang, Y., Cheng, Y., Pei, Q., Wang, C., and Xiang, Y. (2012). Thermal conductivity of defective graphene. Phys. Lett. *376*, 3668–3672.

56. Ng, T., Yeo, J., and Liu, Z. (2012). A molecular dynamics study of the thermal conductivity of graphene nanoribbons containing dispersed stone. Carbon N. Y. *50*, 4887–4893.

57. Yeo, J.J., Liu, Z., and Ng, T.Y. (2012). Comparing the effects of dispersed Stone–Thrower–Wales defects and double vacancies on the thermal conductivity of graphene nanoribbons. Nanotechnology *23*, 385702.

58. Mortazavi, B., and Ahzi, S. (2013). Thermal conductivity and tensile response of defective graphene. Carbon N. Y. *63*, 460–470.

59. Wang, Z.F., Li, Q., Zheng, H., Ren, H., Su, H., Shi, Q.W., and Chen, J. (2007). Tuning the electronic structure of graphene nanoribbons through chemical edge modification. Phys. Rev. B *75*, 113406.

60. Liu, B., Reddy, C., Jiang, J., Baimova, J.A., Dmitriev, S.V., Nazarov, A.A., and Zhou, K. (2012). Morphology and in-plane thermal conductivity of hybrid graphene sheets. Appl. Phys. Lett. *101*, 211909.

61. Chen, S., Wu, Q., Mishra, C., Kang, J., Zhang, H., Cho, K., Cai, W., Balandin, A.A., and Ruoff, R.S. (2012). Thermal conductivity of isotopically modified graphene. Nat. Mater. *11*, 203–207.

62. Mortazavi, B., Rajabpour, A., Ahzi, S., Rémond, Y., and Mehdi Vaez Allaei, S. (2012). Nitrogen doping and curvature effects on thermal conductivity of graphene. Solid State Commun. *152*, 261–264.

63. Song, N., Jiao, D., Cui, S., Hou, X., Ding, P., and Shi, L. (2017). Highly anisotropic thermal conductivity of layer-by-layer assembled nanofibrillated cellulose/graphene nanosheets hybrid films for thermal management. ACS Appl. Mater. Interfaces *9*, 2924–2932.

64. Renteria, J.D., Ramirez, S., Malekpour, H., Alonso, B., Centeno, A., Zurutuza, A., Cocemasov, A.I., Nika, D.L., and Balandin, A.A. (2015). Strongly anisotropic thermal conductivity of free-standing reduced graphene oxide films annealed at high temperature. Adv. Funct. Mater. *25*, 4664–4672.

65. Balandin, A.A. (2011). In-Plane and Cross-Plane Thermal Conductivity of Graphene: Applications in Thermal Interface Materials (SPIE), pp. 7–14.

66. Balandin, A.A. (2014). Phonon engineering in graphene and van der Waals materials. MRS Bull. *39*, 817–823.

67. Prasher, R. (2010). Graphene spreads the heat. Science *328*, 185–186.

68. McClarren, R.G. (2018). Chapter 16 - Gauss quadrature and multi-dimensional integrals. In Computational Nuclear Engineering and Radiological Science Using Python, R.G. McClarren, ed. (Academic Press), pp. 287–299. https://doi.org/10.1016/B978-0-12-812253-2.00018-2.

69. Venkateshan, S.P., and Swaminathan, P. (2014). Chapter 9 - numerical integration. In Computational Methods in Engineering, S.P. Venkateshan and P. Swaminathan, eds. (Academic Press), pp. 317–373. https://doi.org/10.1016/B978-0-12-416702-5.50009-0.

STAR★METHODS

KEY RESOURCES TABLE

REAGENT or RESOURCE	SOURCE	IDENTIFIER
Software and Algorithms		
MATLABMatlab R2019a	MathWorks	www.mathworks.com
COMSOL Multiphysics® Version 5.6	COMSOL	www.comsol.com

RESOURCE AVAILABILITY

Lead contact

Further information and requests should be directed to and will be fulfilled by the Lead Contact, He Tian (tianhe88@tsinghua.edu.cn).

Materials availability

The study did not generate any new materials.

Data and code availability

- All data will be shared upon request to the lead contact.
- This paper does not report original code.
- Any additional analysis information for this work is available by request to the lead contact.

METHOD DETAILS

We constructed the overlapping graphene homojunction model using COMSOL Multiphysics® Version 5.6, and conducted the iterative simulations controled by COMSOL-MATLAB co-programming. The simulations are repeated under different boundary conditions to achieve the NDTR effect at macro scale.

QUANTIFICATION AND STATISTICAL ANALYSIS

No statistical analysis is used.